machines

Article

Dynamic Modeling and Performance Evaluation of a 5-DOF Hybrid Robot for Composite Material Machining

Xiaojian Wang [1,2], Jun Wu [1,2,*] and Yulin Zhou [3]

[1] State Key Laboratory of Tribology in Advanced Equipment, Department of Mechanical Engineering, Institute of Manufacturing Engineering, Tsinghua University, Beijing 100084, China
[2] Beijing Key Lab of Precision/Ultra-Precision Manufacturing Equipment and Control, Beijing 100084, China
[3] College of Mechanical Engineering, Yanshan University, Qinhuangdao 066004, China
* Correspondence: jhwu@mail.tsinghua.edu.cn

Abstract: Dynamic performance is an important performance of robots used for machine processing. This paper studies the dynamic modeling and evaluation method of a 5-DOF (Degree of Freedom) hybrid robot used in aerospace composite material processing. With the consideration of the dynamics of the serial part, the complete dynamic model of the hybrid robot is established based on the virtual work principle. In addition to the widely considered acceleration term, a dynamic performance evaluation index that comprehensively considers the acceleration term, velocity term and gravity term in the dynamic model is proposed. Using the dynamic performance index, the effect of the placement direction of the robot and the arrangement of the double symmetric limbs on robot dynamics are investigated. The results indicate that the vertical placement is beneficial to the dynamics of the hybrid robot, and the arrangement of double symmetric limbs has different effects on different limbs.

Keywords: hybrid robot; kinematics; dynamics; performance evaluation; placement direction

Citation: Wang, X.; Wu, J.; Zhou, Y. Dynamic Modeling and Performance Evaluation of a 5-DOF Hybrid Robot for Composite Material Machining. *Machines* **2023**, *11*, 652. https://doi.org/10.3390/machines11060652

Academic Editors: Zhaokun Zhang, Qizhi Meng and Zhiwei Cui

Received: 4 May 2023
Revised: 7 June 2023
Accepted: 8 June 2023
Published: 16 June 2023

1. Introduction

Because of high stiffness and good bearing capacity, parallel mechanisms have wide application prospects in the machining field [1–4]. Despite these advantages, parallel mechanisms also have the obvious disadvantage of poor dexterity and small workspace [5–8]. Redundancy has been shown to improve the mechanical performance of parallel mechanisms, but control challenges also arise with the introduction of redundancy [9]. On the contrary, serial robots generally have the advantages of good dexterity and a big workspace. The hybrid robot with the merits of both parallel robot and serial robot has great potential in polishing operation [10], pose adjusting system [11], prosthesis and external exoskeleton [12], machining field [13–15], etc. One of the most representative hybrid robots is the 5-DOF hybrid robot that consists of a 3-DOF 2R1T (two rotational DOFs and one translational DOF) parallel mechanism and a 2-DOF serial rotating head, such as the Ecospeed [16], Exechon [17] and Tricept [18,19] robots.

Dynamic performance is of great importance for the robots, especially when the robots are applied in machining field, which requires high dynamic performance [20,21]. It is necessary to establish a dynamic model to study the dynamic performance. However, the hybrid robot not only combines the merits of serial and parallel mechanisms but also inherits their complexity of kinematics [22]. Due to the complex kinematics, the velocity and acceleration of the hybrid robot are generally difficult to be obtained such that it is difficult to establish a complete dynamic model of the hybrid robot. Numerical techniques can be used to obtain the dynamic model of a hybrid robot, but numerical methods generally have poor computational performance [23,24]. In general, only the dynamics of the parallel mechanism in the hybrid robot are considered [25–28]. Han et al. [29] proposed a gain scheduling method based on the dynamic characteristics of the hybrid robot and reduced the overshoot and tracking error. Considering that the driving force of the actuated joints in the serial wrist is weakly coupled with its motion, only the dynamics of the parallel mechanism are taken into consideration. However, the dynamics of the parallel mechanism cannot completely reflect the dynamics of the entire hybrid robot. In order to obtain accurate dynamic characteristics, it is necessary to derive a complete dynamic model of the hybrid robot.

To evaluate the dynamic performance, some dynamic evaluation indices have been presented and they can mainly be classified into two types: ellipsoidal description methods and non-ellipsoidal description methods [30]. The two most classical ellipsoidal description methods are the general inertia ellipsoid (GIE) [31] and the dynamics manipulability ellipsoid (DME) [32]. The GIE represents the easiness of inducing an end-effector velocity with a fixed force, and the DME indicates the easiness of producing an end-effector acceleration by a given set of driving forces. Rao et al. [28] utilized DME to define two performance indices to measure the rotational and translational dynamic characteristics of the 2UPR-PRU (where U, P, and R represent universal, prismatic, and rotating joints, respectively) parallel mechanism. Chen et al. [33] classified the DME into a pure translational DME and a pure rotary DME. A special index was further developed to describe the relationship between the dynamic performances and its pure-translational DOFs. The non-ellipsoidal description method is also a kind of method to describe dynamic performance. Kim and Desa [34] used the acceleration sets to analyze the dynamic performance of a mechanism. Bowing and Kim [35] used dynamic capability hypersurface to analyze the dynamic performance of a mechanism. Xie et al. [36] used the ratio of non-diagonal elements to diagonal elements of the inertia matrix to evaluate the coupling effect of limbs. Most of these evaluation indices generally ignore velocity and gravity in a dynamic model, which will affect the dynamic evaluation. Zhao et al. [37] considered the velocity terms and gravity of the dynamic model when evaluating the dynamic performance of a redundant parallel mechanism. However, there has been no report on the application of evaluation methods considering gravity and velocity in hybrid robots.

In this paper, a complete and analytical dynamic model of the hybrid robot is established, and a dynamic evaluation index that comprehensively considers the acceleration term, velocity term, and gravity term in the dynamic model is proposed. By using the dynamic performance index, the impact of the placement direction of the robot and the arrangement of the double symmetric limbs on the performance of the robot is studied. The rest of this paper is organized as follows: The inverse kinematic model of the hybrid robot is formulated in Section 2. Section 3 establishes the inverse dynamic model of the hybrid robot, and a comprehensive dynamic evaluation index is presented in Section 4. Section 5 studies the effect of the robot placement direction and the arrangement of the double symmetric limbs on dynamic performance. In Section 6, some conclusions are summarized.

2. Inverse Kinematic Analysis

2.1. Structure Description

Figure 1 shows a 5-DOF hybrid robot that is used to machine aerospace structural components with composite material. It consists of a 2-DOF RR rotating head and a 3-DOF 2UPU/SP (where S represents spherical joints) parallel mechanism. The schematic diagram of the robot is shown in Figure 2. As shown in Figure 2a, the 2UPU/SP parallel mechanism consists of a fixed base, three limbs, and a moving platform (MP). Limb 1 and limb 2 are driven by prismatic (P) joints and connected with the MP and the base through universal (U) joints. Limb 3 is driven by a prismatic joint and connected with the base through a spherical (S) joint. The MP is rigidly attached to limb 3. The 2-DOF RR rotating head consists of two rotating joints. As Figure 2 shows, component 4 in RR rotating head is attached to the MP through a rotating joint whose axis is parallel to limb 3. Component 5 in RR rotating head is connected to component 4 through a rotating joint whose axis is perpendicular to the axis of the previous rotating joint.

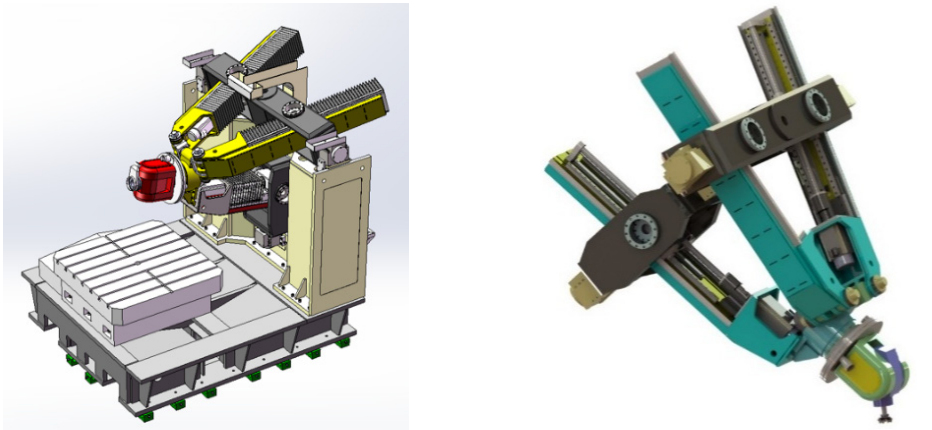

(**a**) (**b**)

Figure 1. 5-DOF hybrid robot [38]: (**a**) 3D model of the hybrid robot; (**b**) 2UPU/SP-RR mechanism.

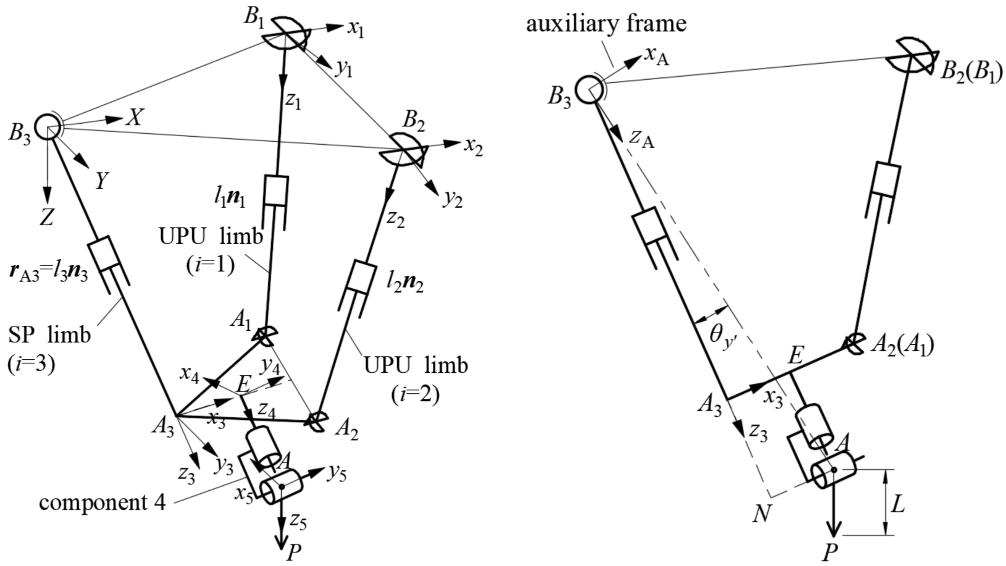

(**a**) (**b**)

Figure 2. Schematic diagram of 2UPU/SP-RR hybrid robot: (**a**) schematic diagram of the hybrid robot; (**b**) auxiliary frame.

As Figure 2a shows, B_i (i = 1, 2) denotes the center of the U joints attached to the base, B_3 denotes the center of the S joint, and A_i (i = 1, 2) denotes the center of the U joints connecting the MP. A_3 denotes the intersection of the SP limb and the plane where A_i (i = 1, 2) are located and SP limb is perpendicular to the plane determined by A_i (i = 1, 2, 3). Triangles $\Delta A_1A_2A_3$ and $\Delta B_1B_2B_3$ are isosceles and similar. In the rotating head, E represents the intersection of the axis of the first rotating joint of the rotating head and the plane spanned by A_i (i = 1, 2, 3), A represents the intersection of the two rotating axes of the rotating head and P represents the end point of end-effector. Fixed frame B_3-XYZ is established at point B_3 with the Y axis parallel to the line B_1B_2 and X axis pointing to the midpoint of the line B_1B_2. Besides, body fixed frame B_i-$x_iy_iz_i$ (i = 1, 2), A_3-$x_3y_3z_3$, E-$x_4y_4z_4$ and A-$x_5y_5z_5$ are established. Frame B_i-$x_iy_iz_i$ (i = 1, 2) is attached to point B_i with z_i axis pointing from B_i to A_i and y_i axis coincident with the first axis of the U joint. Frame A_3-$x_3y_3z_3$ is established at A_3 with z_3 axis coincident with the line B_3A_3 and x_3 axis pointing to the midpoint of the line A_1A_2. In E-$x_4y_4z_4$, y_4 axis is parallel to the axis of the second rotating joint of the rotating head, and z_4 axis is coincident with the line EA. In A-$x_5y_5z_5$, the z_5 axis points from A to P, and the y_5 axis coincides with the axis of the second joint of the rotating head. In addition, the axes not mentioned in the aforementioned frames satisfy the right-hand rule.

2.2. Inverse Position Analysis

2.2.1. Position Analysis of the Parallel Mechanism

For the inverse kinematics of the 5-DOF hybrid robot, the position and posture of the end-effector are given. The position vector of the end point can be represented by $\boldsymbol{r}_P = (x_p \quad y_p \quad z_p)^{\mathrm{T}}$ and the posture of the end-effector can be expressed by two rotation angles α and β. The position vector of A, which is denoted by $\boldsymbol{r}_A = (x_A \quad y_A \quad z_A)^{\mathrm{T}}$, can be obtained as

$$\boldsymbol{r}_A = \boldsymbol{r}_P - L\boldsymbol{n}_P \tag{1}$$

where L represents the distance from points A to P, $\boldsymbol{n}_P$ is the orientation vector of the end-effector and $\boldsymbol{n}_P = \begin{bmatrix}\sin\beta & -\sin\alpha\cos\beta & \cos\alpha\cos\beta\end{bmatrix}^{\mathrm{T}}$. According to the geometric relationship, the length of limb 3 can be written as

$$l_3 = \sqrt{{x_A}^2 + {y_A}^2 + {z_A}^2 - d^2} - k \tag{2}$$

where d represents the distance from point A_3 to E and k represents the distance from E to A.

As Figure 2b shows, an auxiliary frame B_3-$x_A y_A z_A$ is established with z_A axis pointing from B_3 to A, y_A axis parallel to the y_3 axis of A_3-$x_3y_3z_3$, and x_A axis satisfying the right-hand rule. The rotation matrix of auxiliary frame B_3-$x_A y_A z_A$ can be expressed by XYZ Euler angles: firstly rotate θ_{Ax} about X-axis of the local frame; secondly rotate θ_{Ay} about the Y-axis of the new frame; finally rotate θ_{Az} about the Z-axis of the new frame. Based on the B_3-$x_A y_A z_A$, the rotation matrix of A_3-$x_3y_3z_3$ can be obtained by rotating $\theta_{y'}$ around the y_A axis as [38]

$$\boldsymbol{R}_3 = \boldsymbol{R}_{\theta_{Ax}}\boldsymbol{R}_{\theta_{Ay}}\boldsymbol{R}_{\theta_{Az}}\boldsymbol{R}_{\theta_{y'}} \tag{3}$$

where $\boldsymbol{R}_{\theta_{Ax}}$ represents the rotation matrix of angle θ_{Ax}. According to Figure 2b, $\theta_{y'}$ can be obtained as

$$\theta_{y'} = \arcsin(\frac{-d}{l_A}) \tag{4}$$

where $l_A = \sqrt{{x_A}^2 + {y_A}^2 + {z_A}^2}$. The position vector of point A can be written as

$$\boldsymbol{r}_A = \boldsymbol{R}_A\begin{bmatrix}0 & 0 & l_A\end{bmatrix}^{\mathrm{T}} = \begin{bmatrix}l_A\sin\theta_{Ay} & -l_A\sin\theta_{Ax}\cos\theta_{Ay} & l_A\cos\theta_{Ax}\cos\theta_{Ay}\end{bmatrix}^{\mathrm{T}} \tag{5}$$

Based on Equation (5), the angles θ_{Ax} and θ_{Ay} can be expressed as

$$\theta_{Ax} = \arctan\left(-\frac{y_A}{z_A}\right),\ \theta_{Ay} = \arcsin\left(\frac{x_A}{l_A}\right) \tag{6}$$

The angle θ_{Az} must satisfy the structural constraint of plane $A_1A_2B_2B_1$ [39]. The plane constraint can be expressed as

$$(\boldsymbol{r}_{A2} - \boldsymbol{r}_{A1}) \times (\boldsymbol{r}_{B1} - \boldsymbol{r}_{A1}) \cdot (\boldsymbol{r}_{B2} - \boldsymbol{r}_{A1}) = 0 \tag{7}$$

where $\boldsymbol{r}_{A1} = \boldsymbol{r}_{A3} + \boldsymbol{R}_3\begin{bmatrix}p_2 & -q_2 & 0\end{bmatrix}^{\mathrm{T}}$, $\boldsymbol{r}_{A2} = \boldsymbol{r}_{A3} + \boldsymbol{R}_3\begin{bmatrix}p_2 & q_2 & 0\end{bmatrix}^{\mathrm{T}}$, $\boldsymbol{r}_{A3} = \boldsymbol{R}_3\begin{bmatrix}0 & 0 & l_3\end{bmatrix}^{\mathrm{T}}$, $\boldsymbol{r}_{B1} = \begin{bmatrix}p_1 & -q_1 & 0\end{bmatrix}^{\mathrm{T}}$, $\boldsymbol{r}_{B2} = \begin{bmatrix}p_1 & q_1 & 0\end{bmatrix}^{\mathrm{T}}$, p_1 and p_2 are the height of the base side of $\Delta B_1B_2B_3$ and $\Delta A_1A_2A_3$, and q_1 and q_2 are the half of the base side of $\Delta B_1B_2B_3$ and $\Delta A_1A_2A_3$. Based on Equations (3), (4), (6) and (7), the following equation can be obtained

$$\begin{aligned} &z_A l_A({l_3}^2 + kl_3 + p_2 d - p_1 x_A)\sin\theta_{Az} + y_A(p_1{l_A}^2 - x_A{l_3}^2 - kx_A l_3 - p_2 d x_A)\cos\theta_{Az} \\ &= y_A l_{Ayz}(p_2 l_3 + p_2 k - d l_3) \end{aligned} \tag{8}$$

where $l_{Ayz} = \sqrt{{y_A}^2 + {z_A}^2}$. θ_{Az} can be determined by Equation (8)

$$\theta_{Az} = \arcsin\left(\frac{h_3}{\sqrt{{h_1}^2 + {h_2}^2}}\right) - \arctan\left(\frac{h_2}{h_1}\right) \tag{9}$$

where $h_1 = z_A l_A({l_3}^2 + kl_3 + p_2 d - p_1 x_A)$, $h_2 = y_A(p_1 {l_A}^2 - x_A {l_3}^2 - kx_A l_3 - p_2 dx_A)$, $h_3 = y_A l_{Ayz}(p_2 l_3 + p_2 k - dl_3)$.

The position vector of point A_3 can be expressed by

$$\boldsymbol{r}_{A3} = \boldsymbol{R}_3 \begin{bmatrix} 0 & 0 & l_3 \end{bmatrix}^{\mathrm{T}} \tag{10}$$

The closed-loop constraint equation of limbs 1 and 2 can be obtained as

$$\boldsymbol{r}_{A3} = \boldsymbol{b}_i + l_i \boldsymbol{n}_i - \boldsymbol{a}_i, i = 1, 2 \tag{11}$$

where $\boldsymbol{n}_i$ and l_i denote the unit vector and length of the limb i; $\boldsymbol{b}_i$ is the position vector of B_i; $\boldsymbol{a}_i = \boldsymbol{R}_3 {}^3\boldsymbol{a}_i$ and ${}^3\boldsymbol{a}_i$ is the position vector of A_i in A_3-$x_3y_3z_3$. Based on Equations (10) and (11), l_i and $\boldsymbol{n}_i$ can be written as

$$l_i = |\boldsymbol{r}_{A3} - \boldsymbol{b}_i + \boldsymbol{a}_i|,\ \boldsymbol{n}_i = (\boldsymbol{r}_{A3} - \boldsymbol{b}_i + \boldsymbol{a}_i)/l_i,\ i = 1, 2 \tag{12}$$

For limbs 1 and 2, the rotation matrix of B_i-$x_iy_iz_i$ can be described by two rotations: first rotate θ_{iy} about Y-axis of the local frame; then rotate θ_{ix} about the new X-axis. The rotation matrix of B_i-$x_iy_iz_i$ (i = 1, 2) can be obtained as $\boldsymbol{R}_i = \boldsymbol{R}_{\theta_{iy}} \boldsymbol{R}_{\theta_{ix}}$. Then $\boldsymbol{n}_i$ can be also expressed as

$$\boldsymbol{n}_i = \boldsymbol{R}_i \boldsymbol{e}_{3,3} = \begin{bmatrix} \sin\theta_{iy}\cos\theta_{ix} & -\sin\theta_{ix} & \cos\theta_{iy}\cos\theta_{ix} \end{bmatrix}^{\mathrm{T}} \tag{13}$$

where $\boldsymbol{e}_{j,i}$ denotes a j-dimensional column vector in which the i-th element is 1 and the other elements are 0. The angle θ_{iy} and θ_{ix} can be obtained by Equation (13) as

$$\theta_{iy} = \arctan\left(\frac{n_{ix}}{n_{iz}}\right),\ \theta_{ix} = \arcsin(-n_{iy}) \tag{14}$$

2.2.2. Position Analysis of the Rotating Head

For the serial rotating head, the angle of the first rotating joint is represented by φ_z, and the angle of the second rotating joint is denoted by φ_y. The orientation vector of the end-effector can be obtained as

$$\boldsymbol{n}_P = \boldsymbol{R}_3 \boldsymbol{R}_{\varphi_z} \boldsymbol{R}_{\varphi_y} \boldsymbol{e}_{3,3} \tag{15}$$

The joint angles of the rotating head can be obtained by Equation (15) as

$$\varphi_y = \pm\arccos(k_3) \tag{16}$$

$$\varphi_z = \arg\left(\frac{k_1}{\sin\varphi_y} + j\frac{k_2}{\sin\varphi_y}\right) \tag{17}$$

where $k_i = ({\boldsymbol{R}_3}^{\mathrm{T}} \boldsymbol{n}_P) \cdot \boldsymbol{e}_{3,i} = (\boldsymbol{R}_3 \boldsymbol{e}_{3,i})^{\mathrm{T}} \boldsymbol{n}_P (i = 1, 2, 3)$, arg(z) represents the principal argument angle of the complex number z, and j is the imaginary unit. There are two solutions of φ_y of Equation (16), and the solution of φ_y is selected according to the motion trajectory.

2.3. Inverse Velocity Analysis

2.3.1. Velocity Analysis of the Parallel Mechanism

Based on the principle of angular velocity superposition and Equation (3), the angular velocity of limb 3 can be written as

$$\boldsymbol{\omega}_3 = \boldsymbol{e}_{3,1}\dot{\theta}_{Ax} + \boldsymbol{R}_{\theta_{Ax}}\boldsymbol{e}_{3,2}\dot{\theta}_{Ay} + \boldsymbol{R}_{\theta_{Ax}}\boldsymbol{R}_{\theta_{Ay}}\boldsymbol{e}_{3,3}\dot{\theta}_{Az} + \boldsymbol{R}_{\theta_{Ax}}\boldsymbol{R}_{\theta_{Ay}}\boldsymbol{R}_{\theta_{Az}}\boldsymbol{e}_{3,2}\dot{\theta}_{y'} = \boldsymbol{J}_{a3}\dot{\boldsymbol{\Theta}}_3 \tag{18}$$

where $\dot{\boldsymbol{\Theta}}_3 = \begin{bmatrix}\dot{\theta}_{Ax} & \dot{\theta}_{Ay} & \dot{\theta}_{Az} & \dot{\theta}_{yt}\end{bmatrix}^{\mathrm{T}}$, $\boldsymbol{J}_{a3} = \begin{bmatrix}\boldsymbol{e}_{3,1} & \boldsymbol{R}_{\theta_{Ax}}\boldsymbol{e}_{3,2} & \boldsymbol{R}_{\theta_{Ax}}\boldsymbol{R}_{\theta_{Ay}}\boldsymbol{e}_{3,3} & \boldsymbol{R}_{\theta_{Ax}}\boldsymbol{R}_{\theta_{Ay}}\boldsymbol{R}_{\theta_{Az}}\boldsymbol{e}_{3,2}\end{bmatrix}^{\mathrm{T}}$. It can be seen from Equations (4) and (6) that the angles θ_{Ax}, θ_{Ay} and $\theta_{y'}$ are functions of x_A, y_A and z_A. Taking the time derivative of Equations (4) and (6) yields

$$\dot{\theta}_{y'} = \boldsymbol{J}_{\theta_{y'}}\dot{\boldsymbol{r}}_A,\ \dot{\theta}_{Ax} = \boldsymbol{J}_{\theta_{Ax}}\dot{\boldsymbol{r}}_A,\ \dot{\theta}_{Ay} = \boldsymbol{J}_{\theta_{Ay}}\dot{\boldsymbol{r}}_A \tag{19}$$

where

$$\boldsymbol{J}_{\theta_{y'}} = \begin{bmatrix}\frac{\partial\theta_{y'}}{\partial x_A} & \frac{\partial\theta_{y'}}{\partial y_A} & \frac{\partial\theta_{y'}}{\partial z_A}\end{bmatrix} = \begin{bmatrix}\frac{x_A d}{l_A{}^2\sqrt{l_A{}^2-d^2}} & \frac{y_A d}{l_A{}^2\sqrt{l_A{}^2-d^2}} & \frac{z_A d}{l_A{}^2\sqrt{l_A{}^2-d^2}}\end{bmatrix}$$

$\boldsymbol{J}_{\theta_{Ax}}$ and $\boldsymbol{J}_{\theta_{Ay}}$ are given in the Appendix A. It can be seen from Equations (2), (4), (8) and (9) that the angle θ_{Az} can be expressed as a function of h_1, h_2 and h_3; auxiliary variables h_1, h_2 and h_3 are functions of l_A, l_3, l_{Ayz}, x_A, y_A and z_A; l_A, l_3 and l_{Ayz} are functions of x_A, y_A and z_A. Taking time derivative of Equation (9) yields

$$\dot{\theta}_{Az} = \boldsymbol{J}_{\theta_{Az}1}\boldsymbol{h} = \boldsymbol{J}_{\theta_{Az}1}\boldsymbol{J}_{\theta_{Az}2}\begin{bmatrix}\dot{l}_A\dot{l}_3\dot{l}_{Ayz}\dot{x}_A\dot{y}_A\dot{z}_A\end{bmatrix}^T = \boldsymbol{J}_{\theta_{Az}}\dot{\boldsymbol{r}}_A \tag{20}$$

where $\boldsymbol{J}_{\theta_{Az}} = \boldsymbol{J}_{\theta_{Az}1}\boldsymbol{J}_{\theta_{Az}2}\boldsymbol{J}_{\theta_{Az}3}$, $\boldsymbol{J}_{\theta_{Az}1} = \begin{bmatrix}\frac{\partial\theta_{Az}}{\partial h_1} & \frac{\partial\theta_{Az}}{\partial h_2} & \frac{\partial\theta_{Az}}{\partial h_2}\end{bmatrix}$

$$\boldsymbol{J}_{\theta_{Az}2} = \begin{bmatrix}\frac{\partial h_1}{\partial l_A} & \frac{\partial h_1}{\partial l_3} & \frac{\partial h_1}{\partial l_{Ayz}} & \frac{\partial h_1}{\partial x_A} & \frac{\partial h_1}{\partial y_A} & \frac{\partial h_1}{\partial z_A}\\ \frac{\partial h_2}{\partial l_A} & \frac{\partial h_2}{\partial l_3} & \frac{\partial h_2}{\partial l_{Ayz}} & \frac{\partial h_2}{\partial x_A} & \frac{\partial h_2}{\partial y_A} & \frac{\partial h_2}{\partial z_A}\\ \frac{\partial h_3}{\partial l_A} & \frac{\partial h_3}{\partial l_3} & \frac{\partial h_3}{\partial l_{Ayz}} & \frac{\partial h_3}{\partial x_A} & \frac{\partial h_3}{\partial y_A} & \frac{\partial h_3}{\partial z_A}\end{bmatrix},\ \boldsymbol{J}_{\theta_{Az}3} = \begin{bmatrix}\frac{\partial l_A}{\partial x_A} & \frac{\partial l_A}{\partial y_A} & \frac{\partial l_A}{\partial z_A}\\ \frac{\partial l_3}{\partial x_A} & \frac{\partial l_3}{\partial y_A} & \frac{\partial l_3}{\partial z_A}\\ \frac{\partial l_{Ayz}}{\partial x_A} & \frac{\partial l_{Ayz}}{\partial y_A} & \frac{\partial l_{Ayz}}{\partial z_A}\\ & \boldsymbol{E}_{3\times3} & \end{bmatrix}$$

$\boldsymbol{J}_{\theta_{Az}1}$, $\boldsymbol{J}_{\theta_{Az}2}$ and $\boldsymbol{J}_{\theta_{Az}3}$ are given in the Appendix A. $\boldsymbol{e}_{3\times3}$ represents a 3×3 identity matrix.

According to Equations (1) and (18)–(20), the angle velocity of limb 3 can be rewritten as

$$\boldsymbol{\omega}_3 = \boldsymbol{J}_{a3}\boldsymbol{J}_{\theta3}\dot{\boldsymbol{r}}_A = \boldsymbol{J}_{\omega3}\dot{\boldsymbol{X}} \tag{21}$$

where $\boldsymbol{J}_{\omega3} = \boldsymbol{J}_{a3}\boldsymbol{J}_{\theta3}\boldsymbol{J}_{AX}$, $\boldsymbol{J}_{\theta3} = \begin{bmatrix}\boldsymbol{J}_{\theta_{Ax}}{}^{\mathrm{T}} & \boldsymbol{J}_{\theta_{Ay}}{}^{\mathrm{T}} & \boldsymbol{J}_{\theta_{Az}}{}^{\mathrm{T}} & \boldsymbol{J}_{\theta_{y'}}{}^{\mathrm{T}}\end{bmatrix}^{\mathrm{T}}$, $\boldsymbol{J}_{AX} = \boldsymbol{J}_P - L\boldsymbol{J}_{np}$, $\boldsymbol{J}_P = \begin{bmatrix}\boldsymbol{E}_{3\times3} & \boldsymbol{0}_{3\times2}\end{bmatrix}$, $\boldsymbol{0}_{3\times2}$ is a 3×2 null matrix, $\dot{\boldsymbol{X}} = \begin{bmatrix}\dot{x}_P & \dot{y}_P & \dot{z}_P & \dot{\alpha} & \dot{\beta}\end{bmatrix}^{\mathrm{T}}$ and $\boldsymbol{J}_{np} = \begin{bmatrix}0 & 0 & 0 & 0 & \cos\beta\\ 0 & 0 & 0 & -\cos\alpha\cos\beta & \sin\alpha\sin\beta\\ 0 & 0 & 0 & -\sin\alpha\cos\beta & -\cos\alpha\sin\beta\end{bmatrix}$.

Taking time derivative of Equation (10) yields

$$\dot{\boldsymbol{r}}_{A3} = \boldsymbol{\omega}_3\times(\boldsymbol{R}_3\boldsymbol{e}_{3,3}l_3) + \boldsymbol{R}_3\boldsymbol{e}_{3,3}\dot{l}_3 = \boldsymbol{J}_{A3}\dot{\boldsymbol{X}} \tag{22}$$

where $\boldsymbol{J}_{A3} = -[(\boldsymbol{R}_3\boldsymbol{e}_{3,3}l_3)\times]\boldsymbol{J}_{\omega3} + \boldsymbol{R}_3\boldsymbol{e}_{3,3}\boldsymbol{J}_3\boldsymbol{J}_{AX}$, $\boldsymbol{J}_3$ is the third row of $\boldsymbol{J}_{\theta_{Az}3}$ and $[(\boldsymbol{R}_3\boldsymbol{e}_{3,3}l_3)\times]$ represents the skew-symmetric matrix of vector $\boldsymbol{R}_3\boldsymbol{e}_{3,3}l_3$. For example, for a vector $\boldsymbol{w} = \begin{bmatrix}w_x & w_y & w_z\end{bmatrix}^{\mathrm{T}}$, its skew-symmetric matrix is defined as $[\boldsymbol{w}\times] = \begin{bmatrix}0 & -w_z & w_y\\ w_z & 0 & -w_x\\ -w_y & w_x & 0\end{bmatrix}$.

Taking the time derivative of Equation (11) leads to

$$\dot{\boldsymbol{r}}_{A3} = \dot{l}_i\boldsymbol{n}_i + l_i\dot{\boldsymbol{n}}_i - \boldsymbol{\omega}_3\times\boldsymbol{a}_i, i = 1,2 \tag{23}$$

Because $\boldsymbol{n}_i$ is a unit vector, $\dot{\boldsymbol{n}}_i \cdot \boldsymbol{n}_i = 0$. Taking the dot product with $\boldsymbol{n}_i$ on both sides of Equation (23) yields

$$\dot{l}_i = \boldsymbol{n}_i^{\mathrm{T}} \dot{\boldsymbol{r}}_{A3} + (\boldsymbol{a}_i \times \boldsymbol{n}_i)^{\mathrm{T}} \boldsymbol{\omega}_3, i = 1, 2 \tag{24}$$

Rewriting $\dot{l}_i (i = 1, 2, 3)$ in matrix form leads to

$$\dot{\boldsymbol{l}} = \boldsymbol{J}_l \dot{\boldsymbol{X}} \tag{25}$$

where $\dot{\boldsymbol{l}} = \begin{bmatrix} \dot{l}_1 & \dot{l}_2 & \dot{l}_3 \end{bmatrix}^{\mathrm{T}}$, $\boldsymbol{J}_l = \begin{bmatrix} (\boldsymbol{n}_1{}^{\mathrm{T}} \boldsymbol{J}_{A3} + (\boldsymbol{a}_1 \times \boldsymbol{n}_1)^{\mathrm{T}} \boldsymbol{J}_{\omega 3})^{\mathrm{T}} & (\boldsymbol{n}_2{}^{\mathrm{T}} \boldsymbol{J}_{A3} + (\boldsymbol{a}_2 \times \boldsymbol{n}_2)^{\mathrm{T}} \boldsymbol{J}_{\omega 3})^{\mathrm{T}} & (\boldsymbol{J}_3 \boldsymbol{J}_{AX})^{\mathrm{T}} \end{bmatrix}^{\mathrm{T}}$.

According to Equations (14) and (23) and the principle of angular velocity superposition, the angular velocity of limb i (i = 1, 2) is given by

$$\boldsymbol{\omega}_i = \boldsymbol{e}_{3,2} \dot{\theta}_{iy} + \boldsymbol{R}_{\theta_{iy}} \boldsymbol{e}_{3,1} \dot{\theta}_{ix} = \boldsymbol{J}_{ai} \dot{\boldsymbol{\Theta}}_i = \boldsymbol{J}_{ai} \boldsymbol{J}_{\theta i} \dot{\boldsymbol{n}}_i = \boldsymbol{J}_{\omega i} \dot{\boldsymbol{X}} \tag{26}$$

where $\boldsymbol{J}_{\omega i} = \boldsymbol{J}_{ai} \boldsymbol{J}_{\theta i} \boldsymbol{J}_{ni}$, $\boldsymbol{J}_{ni} = (\boldsymbol{J}_{A3} - \boldsymbol{n}_i \boldsymbol{J}_{li} - [\boldsymbol{a}_i \times] \boldsymbol{J}_{\omega 3}) / l_i$, $\boldsymbol{J}_{li}$ is the i-th row of $\boldsymbol{J}_l$, $\boldsymbol{J}_{ai} = \begin{bmatrix} \boldsymbol{e}_{3,2} & \boldsymbol{R}_{\theta_{iy}} \boldsymbol{e}_{3,1} \end{bmatrix}$, $\dot{\boldsymbol{\Theta}}_i = \begin{bmatrix} \dot{\theta}_{iy} & \dot{\theta}_{ix} \end{bmatrix}^{\mathrm{T}}$ and

$$\boldsymbol{J}_{\theta i} = \begin{bmatrix} \frac{n_{iz}}{n_{ix}{}^2 + n_{iz}{}^2} & 0 & \frac{-n_{ix}}{n_{ix}{}^2 + n_{iz}{}^2} \\ 0 & \frac{-1}{\sqrt{1 - n_{iy}{}^2}} & 0 \end{bmatrix}$$

2.3.2. Velocity Analysis of the Rotating Head

Taking time derivative of Equations (16) and (17) yields

$$\dot{\boldsymbol{\Phi}} = \begin{bmatrix} \dot{\varphi}_z & \dot{\varphi}_y \end{bmatrix}^{\mathrm{T}} = \boldsymbol{J}_m \dot{\boldsymbol{k}} = \boldsymbol{J}_\varphi \dot{\boldsymbol{X}} \tag{27}$$

where $\dot{\boldsymbol{k}} = \begin{bmatrix} \dot{k}_1 & \dot{k}_2 & \dot{k}_3 \end{bmatrix}^{\mathrm{T}}$ and $\boldsymbol{J}_\varphi = \boldsymbol{J}_m \boldsymbol{J}_k$. The i-th (i = 1, 2, 3) row of $\boldsymbol{J}_k$ can be written as $((\boldsymbol{R}_3 \boldsymbol{e}_{3,i}) \times \boldsymbol{n}_P)^{\mathrm{T}} \boldsymbol{J}_{\omega 3} + (\boldsymbol{R}_3 \boldsymbol{e}_{3,i})^{\mathrm{T}} \boldsymbol{J}_{np}$. When $\varphi_y = \arccos(k_3)$, $\boldsymbol{J}_m$ can be expressed as

$$\boldsymbol{J}_m = \begin{bmatrix} \frac{-k_2}{k_1{}^2 + k_2{}^2} & \frac{k_1}{k_1{}^2 + k_2{}^2} & 0 \\ 0 & 0 & -\frac{1}{\sqrt{1 - k_3{}^2}} \end{bmatrix}$$

When $\varphi_y = -\arccos(k_3)$, the second row of $\boldsymbol{J}_m$ becomes its opposite number.

According to the principle of angular velocity superposition, the angular velocity of component 4 can be obtained as

$$\boldsymbol{\omega}_4 = \boldsymbol{\omega}_3 + \boldsymbol{R}_3 \boldsymbol{e}_{3,3} \dot{\varphi}_z = \boldsymbol{J}_{\omega 4} \dot{\boldsymbol{X}} \tag{28}$$

where $\boldsymbol{J}_{\omega 4} = \boldsymbol{J}_{\omega 3} + \boldsymbol{R}_3 \boldsymbol{e}_{3,3} \boldsymbol{e}_{2,1}{}^{\mathrm{T}} \boldsymbol{J}_\varphi$. Similarly, the angular velocity of component 5 can be expressed as

$$\boldsymbol{\omega}_5 = \boldsymbol{\omega}_4 + \boldsymbol{R}_4 \boldsymbol{e}_{3,2} \dot{\varphi}_y = \boldsymbol{J}_{\omega 5} \dot{\boldsymbol{X}} \tag{29}$$

where $\boldsymbol{J}_{\omega 5} = \boldsymbol{J}_{\omega 4} + \boldsymbol{R}_4 \boldsymbol{e}_{3,2} \boldsymbol{e}_{2,2}{}^{\mathrm{T}} \boldsymbol{J}_\varphi$.

2.4. Inverse Acceleration Analysis

The angle acceleration of limb 3 can be obtained by taking time derivative of Equation (21) as

$$\dot{\boldsymbol{\omega}}_3 = \boldsymbol{J}_{\omega 3} \ddot{\boldsymbol{X}} + \dot{\boldsymbol{J}}_{\omega 3} \dot{\boldsymbol{X}} \tag{30}$$

where $\dot{\boldsymbol{J}}_{\omega 3} = \dot{\boldsymbol{J}}_{a3} \boldsymbol{J}_{\theta 3} \boldsymbol{J}_{AX} + \boldsymbol{J}_{a3} \dot{\boldsymbol{J}}_{\theta 3} \boldsymbol{J}_{AX} + \boldsymbol{J}_{a3} \boldsymbol{J}_{\theta 3} \dot{\boldsymbol{J}}_{AX}$. Equation (18) shows that the elements in $\boldsymbol{J}_{a3}$ are functions of θ_{Ax}, θ_{Ay} and θ_{Az}. Thus, the elements of the i-th row and j-th column in $\boldsymbol{J}_{a3}$ can be expressed as

$$a_{i,j} = a_{i,j}(\theta_{Ax}, \theta_{Ay}, \theta_{Az}) \tag{31}$$

The elements of the i-th row and j-th column in $\dot{J}_{a3}$ can be written as

$$\dot{a}_{i,j} = \frac{\partial a_{i,j}}{\partial \theta_{Ax}}\dot{\theta}_{Ax} + \frac{\partial a_{i,j}}{\partial \theta_{Ay}}\dot{\theta}_{Ay} + \frac{\partial a_{i,j}}{\partial \theta_{Az}}\dot{\theta}_{Az} \tag{32}$$

$\dot{J}_{a3}$ can be obtained by Matlab software developed by MathWorks, Inc., the United States. $\dot{J}_{\theta 3}$ and $\dot{J}_{AX}$ can be obtained through a similar method.

Taking the time derivative of Equation (25) leads to

$$\ddot{l} = J_l\ddot{X} + \dot{J}_l\dot{X} \tag{33}$$

where

$$\dot{J}_l = \begin{bmatrix} (\omega_1 \times n_1)^{\mathrm{T}}J_{A3} + n_1{}^{\mathrm{T}}\dot{J}_{A3} + ((\omega_3 \times a_1) \times n_1)^{\mathrm{T}}J_{\omega 3} + (a_1 \times (\omega_1 \times n_1))^{\mathrm{T}}J_{\omega 3} + (a_1 \times n_1)^{\mathrm{T}}\dot{J}_{\omega 3} \\ (\omega_2 \times n_2)^{\mathrm{T}}J_{A3} + n_2{}^{\mathrm{T}}\dot{J}_{A3} + ((\omega_3 \times a_2) \times n_2)^{\mathrm{T}}J_{\omega 3} + (a_2 \times (\omega_2 \times n_2))^{\mathrm{T}}J_{\omega 3} + (a_2 \times n_2)^{\mathrm{T}}\dot{J}_{\omega 3} \\ \dot{J}_3 J_{AX} + J_3\dot{J}_{AX} \end{bmatrix}$$

$$\begin{aligned} \dot{J}_{A3} = & -[(\omega_3 \times R_3E_{3,3}l_3)\times]J_{\omega 3} - [(R_3E_{3,3}\dot{l}_3)\times]J_{\omega 3} - [(R_3E_{3,3}l_3)\times]\dot{J}_{\omega 3} \\ & +(\omega_3 \times R_3E_{3,3})J_3J_{AX} + R_3E_{3,3}\dot{J}_3J_{AX} + R_3E_{3,3}J_3\dot{J}_{AX} \end{aligned}$$

Differentiating Equation (26) with respect to time leads to

$$\dot{\omega}_i = J_{\omega i}\ddot{X} + \dot{J}_{\omega i}\dot{X} \tag{34}$$

where $\dot{J}_{\omega i} = \dot{J}_{ai}J_{\theta i}J_{ni} + J_{ai}\dot{J}_{\theta i}J_{ni} + J_{ai}J_{\theta i}\dot{J}_{ni}$

$\dot{J}_{ni} = (\dot{J}_{A3} - (\omega_i \times n_i)J_{li} - n_i\dot{J}_{li} - [(\omega_3 \times a_i)\times]J_{\omega 3} - [a_i\times]\dot{J}_{\omega 3} - \dot{l}_iJ_{ni})/l_i$

$\dot{J}_{ai}$ and $\dot{J}_{\theta i}$ can be obtained by a similar method of solving $\dot{J}_{a3}$.

Taking the time derivative of Equation (28) yields

$$\dot{\omega}_4 = J_{\omega 4}\ddot{X} + \dot{J}_{\omega 4}\dot{X} \tag{35}$$

where $\dot{J}_{\omega 4} = \dot{J}_{\omega 3} + (\omega_3 \times R_3e_{3,3})e_{2,1}{}^{\mathrm{T}}J_{\varphi} + R_3e_{3,3}e_{2,1}{}^{\mathrm{T}}\dot{J}_{\varphi}$ and $\dot{J}_{\varphi} = \dot{J}_mJ_k + J_m\dot{J}_k$. $\dot{J}_m$ can be obtained by a similar method of solving $\dot{J}_{a3}$. The i-th (i = 1, 2, 3) row of $\dot{J}_k$ can be obtained as

$$\begin{aligned} \dot{J}_{ki} = \ & ((\omega_3 \times R_3e_{3,i}) \times n_P)^{\mathrm{T}}J_{\omega 3} + ((R_3e_{3,i}) \times \dot{n}_P)^{\mathrm{T}}J_{\omega 3} + ((R_3e_{3,i}) \times n_P)^{\mathrm{T}}\dot{J}_{\omega 3} \\ & +(\omega_3 \times R_3e_{3,i})^{\mathrm{T}}J_{np} + (R_3e_{3,i})^{\mathrm{T}}\dot{J}_{np} \end{aligned}$$

Taking the time derivative of Equation (29) leads to

$$\dot{\omega}_5 = J_{\omega 5}\ddot{X} + \dot{J}_{\omega 5}\dot{X} \tag{36}$$

where $\dot{J}_{\omega 5} = \dot{J}_{\omega 4} + (\omega_4 \times R_4e_{3,2})e_{2,2}{}^{\mathrm{T}}J_{\varphi} + R_4e_{3,2}e_{2,2}{}^{\mathrm{T}}\dot{J}_{\varphi}$.

3. Inverse Dynamic Analysis

The inverse dynamics is to determine the driving force or driving torque with a given motion and external force of the end-effector. To simplify the analysis, the joint inertia is neglected. As Figure 3 shows, the limb of the parallel mechanism can be divided into two components according to the nature of motion. The motion of the first component S_{i1} including the limb body, linear guideway, and motor is a general motion. The motion of the second component S_{i2} including the lead-screw, coupler, and motor rotor is the afore-mentioned motion plus a rotation about the n_i axis. The virtual power of limb i can be obtained as

$$\begin{aligned} \delta P_i = \ & \delta\dot{r}_{Ci}{}^{\mathrm{T}}(m_ig - m_i\ddot{r}_{Ci}) + \delta\omega_i{}^{\mathrm{T}}(-I_i\dot{\omega}_i - \omega_i \times (I_i\omega_i)) \\ & +\delta\omega_{mi}{}^{\mathrm{T}}(-I_{mi}\dot{\omega}_{mi} - \omega_{mi} \times (I_{mi}\omega_{mi})), i = 1, 2, 3 \end{aligned} \tag{37}$$

where $\boldsymbol{I}_i = \boldsymbol{R}_i \boldsymbol{I}'_i \boldsymbol{R}_i^{\mathrm{T}}$ and $\boldsymbol{I}'_i$ is the inertia matrix of S_{i1} with respect to the centroid; $\boldsymbol{I}_{mi} = \boldsymbol{R}_i \boldsymbol{I}'_{mi} \boldsymbol{R}_i^{\mathrm{T}}$ and $\boldsymbol{I}'_{mi}$ is the inertia matrix of S_{i2} with respect to the centroid; $\boldsymbol{g}$ represents the gravitational acceleration; m_i represents the mass of S_{i1} and S_{i2} as a whole; $\dot{\boldsymbol{r}}_{Ci}$ and $\ddot{\boldsymbol{r}}_{Ci}$ are the velocity and acceleration of the centroid of limb i which is denoted by C_i; $\boldsymbol{\omega}_{mi}$ and $\dot{\boldsymbol{\omega}}_{mi}$ represent the angular velocity and acceleration of S_{i2}. According to Figure 3, we can obtain

$$\boldsymbol{r}_{C3} = (l_3 - e_3)\boldsymbol{n}_3,\ \boldsymbol{r}_{Ci} = \boldsymbol{b}_i + (l_i - e_i)\boldsymbol{n}_i,\ i = 1,2 \tag{38}$$

$$\dot{\boldsymbol{r}}_{Ci} = \boldsymbol{J}_{vci}\dot{\boldsymbol{X}}, i = 1,2,3 \tag{39}$$

$$\ddot{\boldsymbol{r}}_{Ci} = \boldsymbol{J}_{vci}\ddot{\boldsymbol{X}} + \dot{\boldsymbol{J}}_{vci}\dot{\boldsymbol{X}}, i = 1,2,3 \tag{40}$$

where $\boldsymbol{J}_{vci} = \boldsymbol{n}_i\boldsymbol{J}_{li} - (l_i - e_i)[\boldsymbol{n}_i\times]\boldsymbol{J}_{\omega i}$, $\boldsymbol{J}_{li}$ represents the i-th row of $\boldsymbol{J}_l$, e_i is the distance from A_i to C_i, $\dot{\boldsymbol{J}}_{vci} = (\boldsymbol{\omega}_i \times \boldsymbol{n}_i)\boldsymbol{J}_{li} + \boldsymbol{n}_i\dot{\boldsymbol{J}}_{li} - \dot{l}_i[\boldsymbol{n}_i\times]\boldsymbol{J}_{\omega i} - (l_i - e_i)([(\boldsymbol{\omega}_i \times \boldsymbol{n}_i)\times]\boldsymbol{J}_{\omega i} + [\boldsymbol{n}_i\times]\dot{\boldsymbol{J}}_{\omega i})$ and $\dot{\boldsymbol{J}}_{li}$ is the i-th row of $\dot{\boldsymbol{J}}_l$. The angular velocity of S_{i2} in B_3-XYZ can be obtained as

$$\boldsymbol{\omega}_{mi} = \boldsymbol{\omega}_i + \frac{2\pi\dot{l}_i}{p_i}\boldsymbol{n}_i = \boldsymbol{J}_{\omega mi}\dot{\boldsymbol{r}}_3, \boldsymbol{J}_{\omega mi} = \boldsymbol{J}_{\omega i} + \frac{2\pi\boldsymbol{n}_i\boldsymbol{J}_{li}}{p_i} \tag{41}$$

where p_i is the pitch of the lead-screw. The angular acceleration of S_{i2} can be obtained by Differentiating Equation (41) with respect to time as

$$\dot{\boldsymbol{\omega}}_{mi} = \boldsymbol{J}_{\omega mi}\ddot{\boldsymbol{r}}_3 + \dot{\boldsymbol{J}}_{\omega mi}\dot{\boldsymbol{r}}_3 \tag{42}$$

where $\dot{\boldsymbol{J}}_{\omega mi} = \dot{\boldsymbol{J}}_{\omega i} + \frac{2\pi(\boldsymbol{\omega}_i\times\boldsymbol{n}_i)\boldsymbol{J}_{li}}{p_i} + \frac{2\pi\boldsymbol{n}_i\dot{\boldsymbol{J}}_{li}}{p_i}$.

The virtual power of the components of the rotating head can be expressed as

$$\delta P_i = \delta\dot{\boldsymbol{r}}_{Ci}{}^{\mathrm{T}}(m_i\boldsymbol{g} - m_i\ddot{\boldsymbol{r}}_{Ci}) + \delta\boldsymbol{\omega}_i{}^{\mathrm{T}}(-\boldsymbol{I}_i\dot{\boldsymbol{\omega}}_i - \boldsymbol{\omega}_i \times (\boldsymbol{I}_i\boldsymbol{\omega}_i)), i = 4,5 \tag{43}$$

where m_i is the mass of component i; $\boldsymbol{I}_i = \boldsymbol{R}_i\boldsymbol{I}'_i\boldsymbol{R}_i^{\mathrm{T}}$ and $\boldsymbol{I}'_i$ is the inertia matrix of component i with respect to the centroid; $\dot{\boldsymbol{r}}_{Ci}$ and $\ddot{\boldsymbol{r}}_{Ci}$ are the velocity and acceleration of the centroid of component i. According to Figure 2, we can obtain

$$\boldsymbol{r}_{C4} = \boldsymbol{r}_{A3} + \boldsymbol{R}_3{}^3\boldsymbol{r}_{C4}, \boldsymbol{r}_{C5} = \boldsymbol{r}_A + \boldsymbol{R}_5{}^5\boldsymbol{r}_{C5} \tag{44}$$

$$\dot{\boldsymbol{r}}_{Ci} = \boldsymbol{J}_{vci}\dot{\boldsymbol{X}}, i = 4,5 \tag{45}$$

$$\ddot{\boldsymbol{r}}_{Ci} = \boldsymbol{J}_{vci}\ddot{\boldsymbol{X}} + \dot{\boldsymbol{J}}_{vci}\dot{\boldsymbol{X}}, i = 4,5 \tag{46}$$

where $\boldsymbol{J}_{vc4} = \boldsymbol{J}_{A3} - [(\boldsymbol{R}_3{}^3\boldsymbol{r}_{C4})\times]\boldsymbol{J}_{\omega 3}$
$\boldsymbol{J}_{vc5} = \boldsymbol{J}_{AX} - [(\boldsymbol{R}_5{}^5\boldsymbol{r}_{C5})\times]\boldsymbol{J}_{\omega 5}$
$\dot{\boldsymbol{J}}_{vc4} = \dot{\boldsymbol{J}}_{A3} - [(\boldsymbol{\omega}_3 \times \boldsymbol{R}_3{}^3\boldsymbol{r}_{C4})\times]\boldsymbol{J}_{\omega 3} - [(\boldsymbol{R}_3{}^3\boldsymbol{r}_{C4})\times]\dot{\boldsymbol{J}}_{\omega 3}$
$\dot{\boldsymbol{J}}_{vc5} = \dot{\boldsymbol{J}}_{AX} - [(\boldsymbol{\omega}_5 \times \boldsymbol{R}_5{}^5\boldsymbol{r}_{C5})\times]\boldsymbol{J}_{\omega 5} - [(\boldsymbol{R}_5{}^5\boldsymbol{r}_{C5})\times]\dot{\boldsymbol{J}}_{\omega 5}$
${}^3\boldsymbol{r}_{C4}$ denotes the position vector of C_4 in A_3-$x_3y_3z_3$ and ${}^5\boldsymbol{r}_{C5}$ is the position vector of C_5 in A-$x_5y_5z_5$.

The virtual work principle yields

$$\sum_{i=1}^{5}\delta P_i + \delta\dot{\boldsymbol{q}}^{\mathrm{T}}\boldsymbol{f} + \delta\dot{\boldsymbol{r}}_P{}^{\mathrm{T}}\boldsymbol{F} + \delta\boldsymbol{\omega}_5{}^{\mathrm{T}}\boldsymbol{T} = 0 \tag{47}$$

where $\boldsymbol{f} = [f_1, f_2, f_3, \tau_4, \tau_5]^{\mathrm{T}}$ represents the actuating force vector, $\boldsymbol{T}$ and $\boldsymbol{F}$ represent the external torque and external force on end-effector with respect to point P, $\delta\dot{\boldsymbol{q}} =$

$[\dot{l}_1 \quad \dot{l}_2 \quad \dot{l}_3 \quad \dot{\varphi}_z \quad \dot{\varphi}_y]^{\mathrm{T}}$, $\delta\dot{\boldsymbol{q}} = \boldsymbol{J}_q\delta\dot{\boldsymbol{X}}$, $\boldsymbol{J}_q = [\boldsymbol{J}_l{}^{\mathrm{T}} \quad \boldsymbol{J}_\varphi{}^{\mathrm{T}}]^{\mathrm{T}}$, $\delta\boldsymbol{v}_P = \boldsymbol{J}_{vp}\delta\dot{\boldsymbol{X}}$ and $\boldsymbol{J}_{vp} = [\boldsymbol{E}_{3\times3} \quad 0_{3\times2}]$. By substituting Equations (37) and (43) into Equation (47), the inverse dynamic equation of the hybrid robot can be written as

$$\boldsymbol{f} = \boldsymbol{f}_a + \boldsymbol{f}_v + \boldsymbol{f}_g \tag{48}$$

where $\boldsymbol{f}_a = \boldsymbol{M}(\boldsymbol{X})\ddot{\boldsymbol{X}}$ represents the acceleration term, $\boldsymbol{f}_v = \boldsymbol{C}(\boldsymbol{X},\dot{\boldsymbol{X}})\dot{\boldsymbol{X}}$ represents the velocity term, $\boldsymbol{f}_g = \boldsymbol{G}(\boldsymbol{X})$ represents the gravity and external force term,

$$\boldsymbol{M} = \boldsymbol{J}_q{}^{-\mathrm{T}}\left[\sum_{i=1}^{5}\left(m_i\boldsymbol{J}_{vci}{}^{\mathrm{T}}\boldsymbol{J}_{vci} + \boldsymbol{J}_{\omega i}{}^{\mathrm{T}}\boldsymbol{I}_i\boldsymbol{J}_{\omega i}\right) + \sum_{i=1}^{3}\left(\boldsymbol{J}_{\omega mi}{}^{\mathrm{T}}\boldsymbol{I}_{mi}\boldsymbol{J}_{\omega mi}\right)\right]$$

$$\boldsymbol{C} = \boldsymbol{J}_q{}^{-\mathrm{T}}\left[\begin{array}{l}\sum\limits_{i=1}^{5}\left(m_i\boldsymbol{J}_{vci}{}^{\mathrm{T}}\dot{\boldsymbol{J}}_{vci} + \boldsymbol{J}_{\omega i}{}^{\mathrm{T}}\boldsymbol{I}_i\dot{\boldsymbol{J}}_{\omega i} - \boldsymbol{J}_{\omega i}{}^{\mathrm{T}}[(\boldsymbol{I}_i\boldsymbol{\omega}_i)\times]\boldsymbol{J}_{\omega i}\right)\\ +\sum\limits_{i=1}^{3}\left(\boldsymbol{J}_{\omega mi}{}^{\mathrm{T}}\boldsymbol{I}_{mi}\dot{\boldsymbol{J}}_{\omega mi} - \boldsymbol{J}_{\omega mi}{}^{\mathrm{T}}[(\boldsymbol{I}_{mi}\boldsymbol{\omega}_{mi})\times]\boldsymbol{J}_{\omega mi}\right)\end{array}\right]$$

$$\boldsymbol{G} = -\boldsymbol{J}_q{}^{-\mathrm{T}}\left(\sum_{i=1}^{5} m_i\boldsymbol{J}_{vci}{}^{\mathrm{T}}\boldsymbol{g} + \boldsymbol{J}_{vp}{}^{\mathrm{T}}\boldsymbol{F} + \boldsymbol{J}_{\omega 5}{}^{\mathrm{T}}\boldsymbol{T}\right)$$

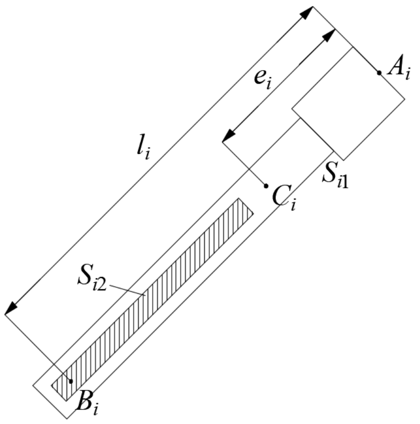

Figure 3. Schematic diagrams of limb structure. Reprinted with permission from ref. [40]. Copyright 2021 Elsevier.

4. Dynamic Performance Evaluation

4.1. Dynamic Performance Indices

For the limbs of the parallel mechanism, for given acceleration and velocity range of the end-effector, the driving force demand of each motor for a specific position and posture of end-effector can be written as

$$f_{i,\min}(\boldsymbol{X}) \leq f_i \leq f_{i,\max}(\boldsymbol{X}), i = 1,2,3 \tag{49}$$

where $f_{i,\min}$ and $f_{i,\max}$ are the minimum and maximum of f_i at the given position and posture. For the same motion of end-effector, a larger absolute value of driving force means higher requirements for the motor, and it will be more difficult to change the velocity and acceleration of end-effector. At the same time, the robot will bear greater internal force, which will have an adverse impact on the accuracy of the robot. Therefore, a larger absolute value of driving force can be considered as a worse working situation, and a local dynamic performance index can be defined as

$$f_{i\max} = \max\{|f_{i,\max}|, |f_{i,\min}|\} \tag{50}$$

Since the $f_{i\max}$ changes with the robot configuration, a global index to evaluate the average dynamic performance of the robot in the workspace can be defined as

$$\overline{f}_{i\max} = \frac{\int\limits_{W_t} f_{i\max} dV}{\int\limits_{W_t} dV} \tag{51}$$

where W_t represents the workspace.

4.2. Task Space and Motion Range of the Hybrid Robot

As shown by the red line in Figure 4, the task workspace of the hybrid robot is a cylinder whose radius is 600 mm. h = 300 mm is the height of the workspace, H = 1650 mm is the distance from O to the upper bound of the workspace and e = 422.5 mm is the distance between the Y to y axes of O-xyz. According to the practical application requirements, the required range of the posture of end-effector is specified as $-20° \leq \alpha \leq 20°$ and $-20° \leq \beta \leq 20°$. To ensure that the robot is not singular in the workspace, we investigate the singularity of matrix $\boldsymbol{M}$ in Equation (48). The distribution of the minimum of determinant of matrix $\boldsymbol{M}$ under the required posture range in the lower layer where z = 1900 mm, middle layer where z = 1800 mm and upper layer where z = 1700 mm of the workspace is shown in Figure 5. It can be seen that the determinant of matrix $\boldsymbol{M}$ is far away from zero in the workspace, so matrix $\boldsymbol{M}$ is nonsingular in the workspace, which ensures the rationality of subsequent analysis.

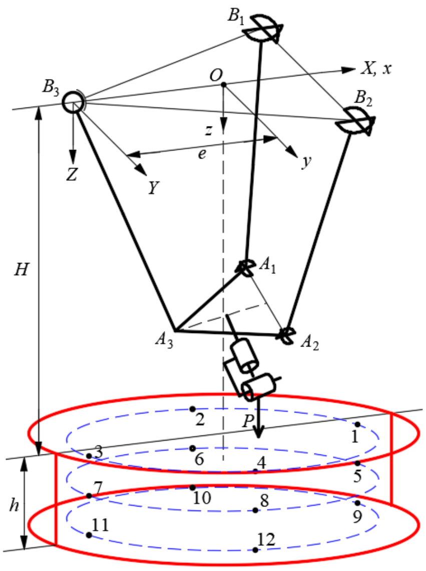

Figure 4. Workspace of the hybrid robot and typical position in the workspace.

The 2UPU/SP-RR hybrid robot has three translational DOFs and two rotational DOFs. In order to calculate the maximum absolute value of driving force at a given position in the workspace, the posture of the end-effector is taken as the limiting condition, whose range is specified as $-20° \leq \alpha \leq 20°$ and $-20° \leq \beta \leq 20°$.

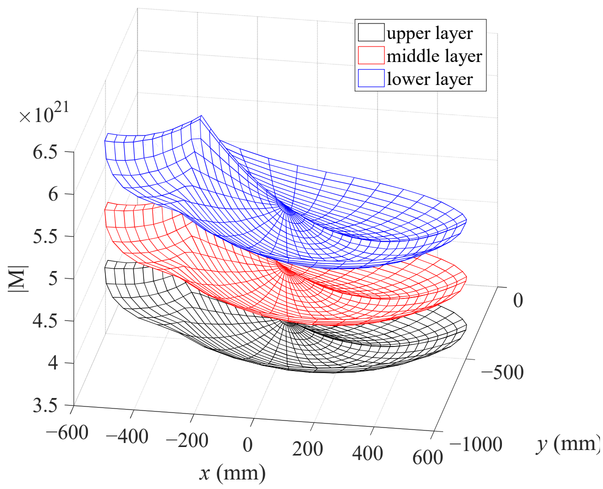

Figure 5. Distribution of minimum of determinant of matrix $\boldsymbol{M}$ under the required posture range in the workspace.

According to Equation (48), the driving force of limb i at a given position can be written as

$$f_i = f_{ai}(\ddot{x}, \ddot{y}, \ddot{z}, \ddot{\alpha}, \ddot{\beta}, \alpha, \beta) + f_{vi}(\dot{x}, \dot{y}, \dot{z}, \dot{\alpha}, \dot{\beta}, \alpha, \beta) + f_{gi}(\alpha, \beta) \tag{52}$$

where $f_{ai} = \boldsymbol{M}_i\ddot{\boldsymbol{X}}$, $f_{vi} = \boldsymbol{C}_i\dot{\boldsymbol{X}}$, $f_{gi} = G_i$, and $\boldsymbol{M}_i$, $\boldsymbol{C}_i$ and G_i are the i-th row of $\boldsymbol{M}$, $\boldsymbol{C}$ and $\boldsymbol{G}$.

It can be seen from Equation (52) that the acceleration term is determined by the acceleration and posture of the end-effector, the velocity term is determined by the velocity and posture of the end-effector, and the gravity and external force term is determined by posture. To simplify the calculation of the maximum absolute value of f_i, the influence of posture on the acceleration and velocity term is investigated. Twelve typical positions are selected on the circle with a radius of 500 mm in the lower layer, middle layer, and upper layer of the workspace, as shown in Figure 4. The distributions of maximum and minimum values of the acceleration and velocity term with posture at these typical positions are calculated by the MultiStart solver of Matlab 2016b. The ratio of the standard deviation to the mean value, which reflects the effect of the posture of the end-effector on the maximum and minimum acceleration and velocity term, is shown in Figure 6.

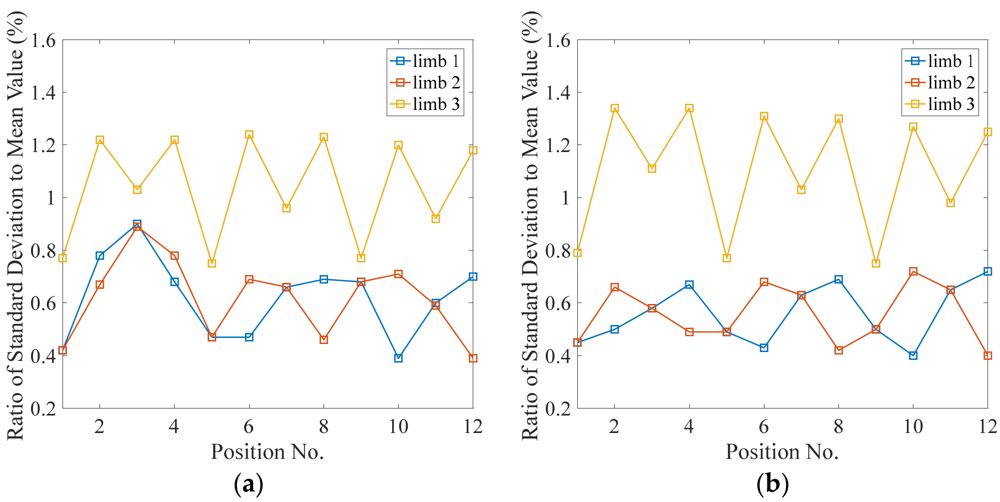

Figure 6. The influence of posture of end-effector on acceleration and velocity term: (**a**) influence on the maximum of acceleration and velocity term; (**b**) influence on the minimum of acceleration and velocity term.

Figure 6 shows that the posture of the end-effector has little effect on the maximums and minimums of acceleration and velocity items. In order to simplify the calculation, the effect of the posture of the end-effector is ignored to calculate the acceleration and velocity item, namely

$$f_i = f_{ai}(\ddot{x}, \ddot{y}, \ddot{z}, \ddot{\alpha}, \ddot{\beta}) + f_{vi}(\dot{x}, \dot{y}, \dot{z}, \dot{\alpha}, \dot{\beta}) + f_{gi}(\alpha, \beta) \tag{53}$$

Then, we can obtain that

$$f_{i,\min} = f_{ai,\min} + f_{vi,\min} + f_{gi,\min},\ f_{i,\max} = f_{ai,\max} + f_{vi,\max} + f_{gi,\max} \tag{54}$$

According to the practical application requirements, the velocity and acceleration requirements of the hybrid robot are given as $|\ddot{x}| \le 2.5\,\mathrm{m/s^2}$, $|\dot{x}| \le 0.5\,\mathrm{m/s}$, $|\ddot{y}| \le 2.5\,\mathrm{m/s^2}$, $|\dot{y}| \le 0.5\,\mathrm{m/s}$, $|\ddot{z}| \le 2.5\,\mathrm{m/s^2}$, $|\dot{z}| \le 0.5\,\mathrm{m/s}$, $|\ddot{\alpha}| \le 0.25\,\mathrm{rad/s^2}$, $|\dot{\alpha}| \le 0.05\,\mathrm{rad/s}$, $|\ddot{\beta}| \le 0.25\,\mathrm{rad/s^2}$, $|\dot{\beta}| \le 0.05\,\mathrm{rad/s}$.

5. Dynamic Performance Comparison

5.1. Influence of Hybrid Robot Placement Direction on Dynamic Performance

In practical application, the hybrid robot can be vertically or horizontally placed as shown in Figure 7. With different placement direction, gravity has a different effect on the dynamic performance. The inertial and geometric parameters of the robot are listed in the Appendix A. The indices f_{gi} (i = 1, 2, 3) and $f_{i\max}$ (i = 1, 2, 3) in the middle layer of the workspace are calculated by the MultiStart solver of Matlab 2016b, as shown in Figures 8 and 9, and $\overline{f}_{i\max}$ is listed in Table 1. Figure 8 shows that when the robot is placed vertically, the motor of a limb needs to provide tension for the gravity term in the workspace near the limb, but to provide thrust in the workspace away from the limb. When the robot is placed horizontally, limbs 1 and 2 always need to provide a greater tension for the gravity term, and limb 3 always needs to provide a greater thrust for the gravity term.

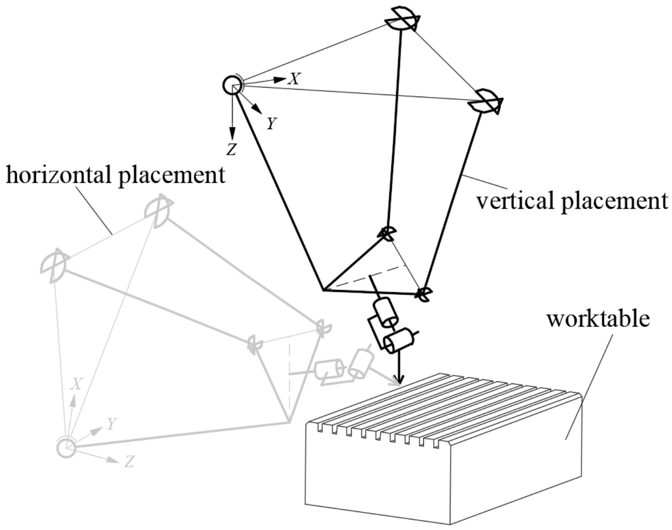

Figure 7. Different placement directions of hybrid robot.

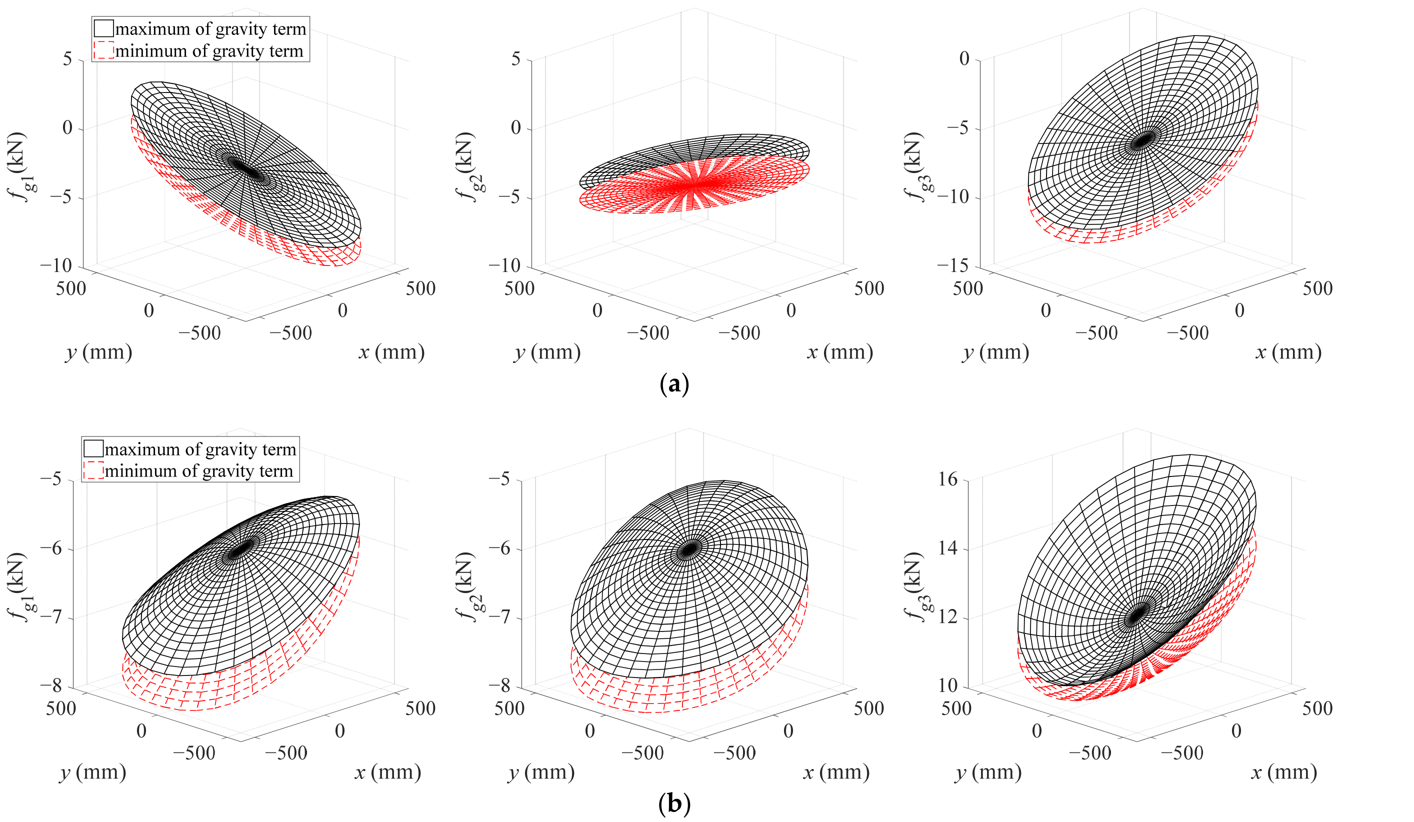

Figure 8. Distributions of gravity term of driving force in the middle layer of the workspace: (**a**) vertical; (**b**) horizontal.

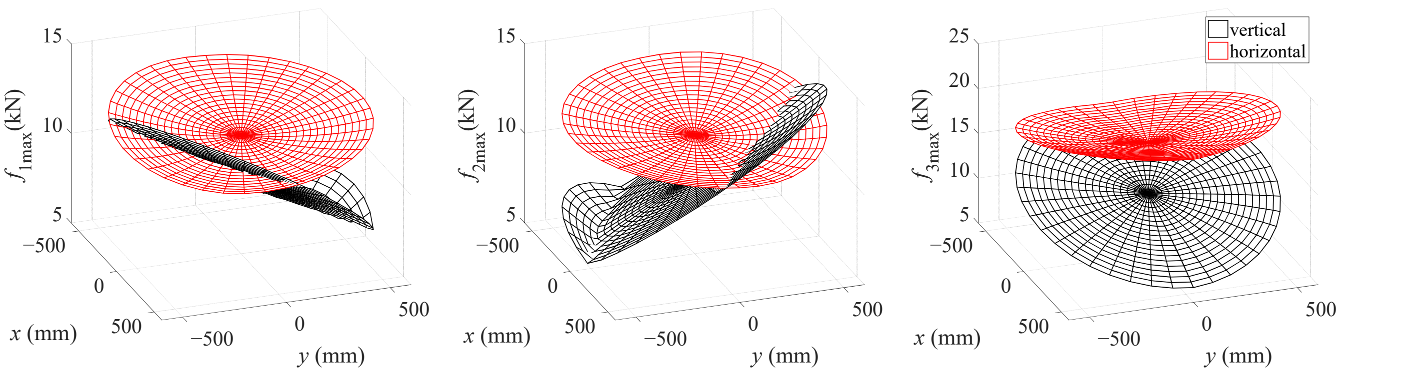

Figure 9. Distributions of $f_{i\max}$ in the middle layer of the workspace in vertical and horizontal placement.

Table 1. Global performance indices in vertical and horizontal placement (unit: kN).

Global Index	Vertical	Horizontal
$\overline{f}_{1\max}$	9.56	12.04
$\overline{f}_{2\max}$	9.56	12.04
$\overline{f}_{3\max}$	11.85	18.62

Figure 9 shows that in most workspaces, a smaller maximum absolute value of driving force is required in vertical placement than in horizontal placement. Only when the end-effector is close to a limb, the maximum absolute value of the driving force of the limb in vertical placement will be greater than that in horizontal placement. The results in Table 1 show that the average maximum absolute value of driving force in vertical placement is smaller, especially $\overline{f}_{3\max}$ is 36.36% less than that in horizontal placement, which indicates that the vertical placement is beneficial to the dynamics of the hybrid robot.

5.2. Effect of the Position of Double Symmetric Limbs on the Dynamic Performance

The arrangement of the limbs in horizontal placement will also affect the dynamic characteristics of the robot. The three limbs of the parallel mechanism in hybrid robot are usually arranged symmetrically due to the symmetrical structure of the mechanism, so there are two cases of double limbs on the top and double limbs on the bottom. The indices f_{gi} (i = 1, 2, 3) and $f_{i\max}$ (i = 1, 2, 3) in the middle layer of the workspace in the two cases are calculated by the MultiStart solver of Matlab 2016b, as shown in Figures 10 and 11, and $\overline{f}_{i\max}$ is listed in Table 2. Figure 10 shows that when the double limbs are on the top, the double limbs need to provide tension for the gravity term of driving force while limb 3 needs to provide thrust for the gravity term of driving force; when the double limbs are on the bottom, the double limbs need to provide thrust for the gravity term of driving force while limb 3 needs to provide tension for the gravity term of driving force.

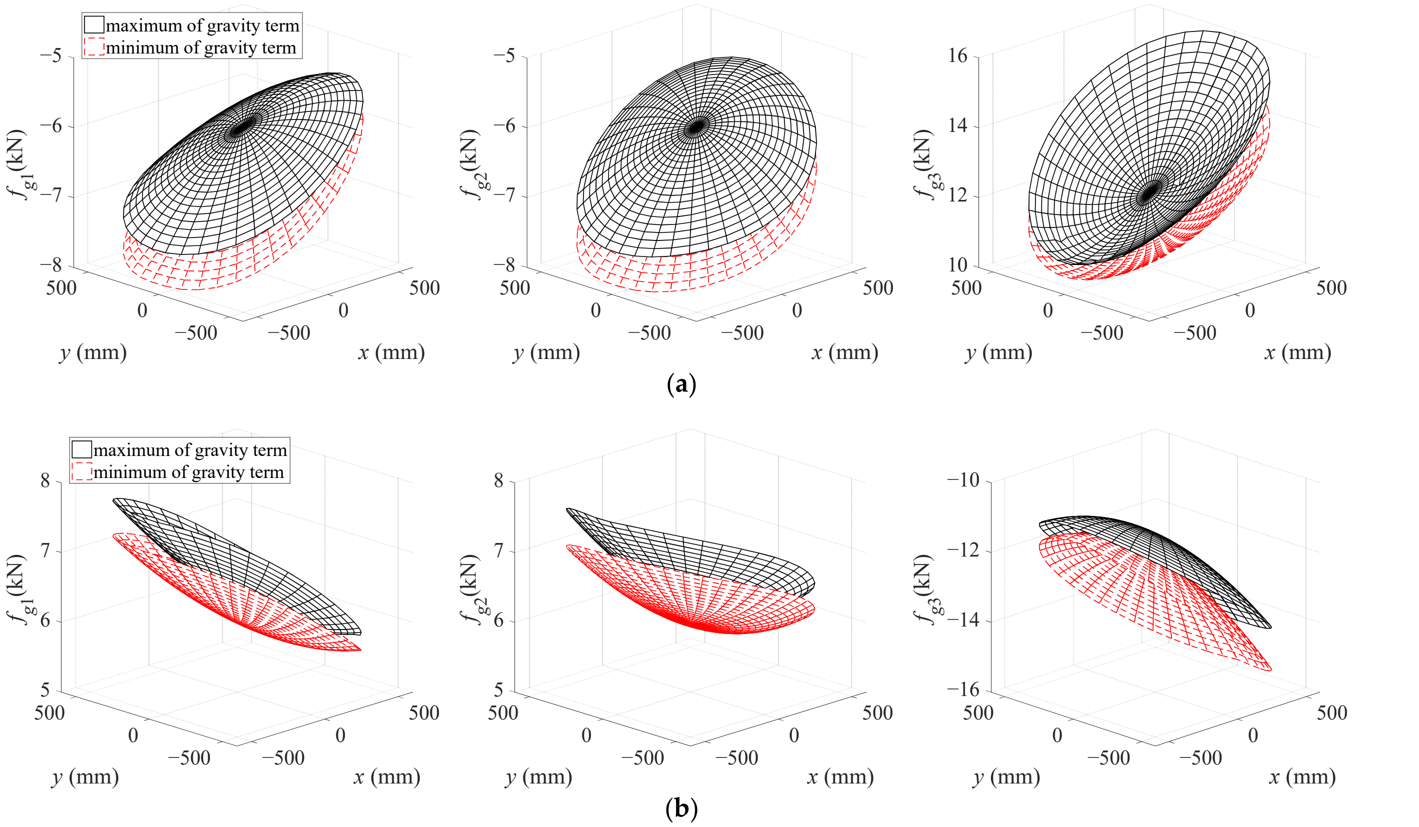

Figure 10. Distributions of gravity term of driving force in the middle layer of the workspace: (**a**) double limbs on the top; (**b**) double limbs on the bottom.

Table 2. Global performance indices in different arrangements of the limbs (unit: kN).

Global index	Double Limbs on the Top	Double Limbs on the Bottom
$\overline{f}_{1\max}$	12.04	12.26
$\overline{f}_{2\max}$	12.04	12.26
$\overline{f}_{3\max}$	18.62	18.36

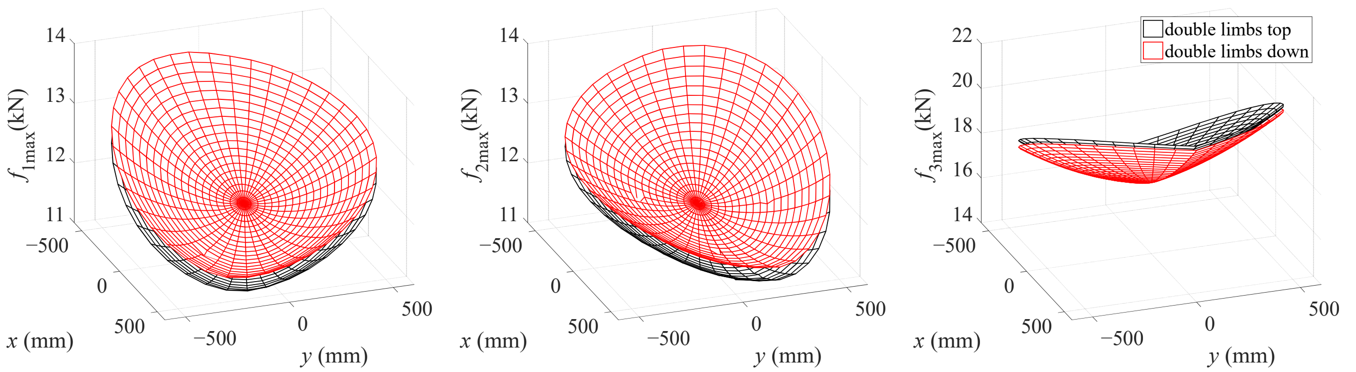

Figure 11. Distributions of $f_{i\max}$ in the middle layer of the workspace in different arrangements of the limbs.

Figure 11 and Table 2 show that when the double limbs are on the top, limbs 1 and 2 require smaller average maximum absolute values of driving force while limb 3 requires larger average maximum absolute values of the driving force, which indicates that the arrangement of the limbs has different effects on the dynamic performance of different limbs. Considering that the double limbs and the worktable or workpiece are prone to interference when the double limbs are on the bottom, the double limbs are often on the top when the robot is placed horizontally in practical application.

6. Conclusions

In this paper, the complete dynamic equation of a 5-DOF hybrid robot is formulated. A dynamic evaluation index taking velocity and gravity terms in the dynamic model into consideration is proposed. Then, the effect of the placement direction of the robot and the arrangement mode of the double symmetric limbs on the dynamics is investigated. The conclusions are drawn as follows:

(1) The maximum absolute value of the driving force of the robot at given motion limits of the end-effector can be regarded as the dynamic evaluation index of the hybrid robot.

(2) The influence of placement direction on the dynamics of the hybrid is investigated, and the results indicate that vertical placement is beneficial to the dynamics of the hybrid robot.

(3) The effect of the position of the double limbs on the dynamic performance is investigated. The results show that when double limbs are arranged on top, the average dynamic performance of the double limbs can be improved, while the dynamic performance of the third limb will be slightly deteriorated.

Author Contributions: Methodology, X.W. and J.W.; formal analysis, X.W. and Y.Z.; writing—original draft preparation, X.W. and J.W.; funding acquisition, J.W. All authors have read and agreed to the published version of the manuscript.

Funding: This research was funded by the National Natural Science Foundation of China (Grant No. 51975321) and EU H2020-MSCA-RISE-ECSASDPE (No. 734272).

Data Availability Statement: All data included in this study are available upon request by contact with the corresponding author.

Acknowledgments: This work was supported Tianjin Key Laboratory of High Speed Cutting and Precision Machining.

Conflicts of Interest: The authors declare no conflict of interest.

Appendix A

The expressions of $\boldsymbol{J}_{\theta_{Ax}}$ and $\boldsymbol{J}_{\theta_{Ay}}$ are

$$\boldsymbol{J}_{\theta_{Ax}} = \begin{bmatrix} 0 & -\frac{z_A}{l_{Ayz}{}^2} & \frac{y_A}{l_{Ayz}{}^2} \end{bmatrix}, \ \boldsymbol{J}_{\theta_{Ay}} = \begin{bmatrix} \frac{l_{Ayz}}{l_A{}^2} & \frac{-x_A y_A}{l_{Ayz} l_A{}^2} & \frac{-x_A z_A}{l_{Ayz} l_A{}^2} \end{bmatrix}$$

The expressions of $\boldsymbol{J}_{\theta_{Az}1}$, $\boldsymbol{J}_{\theta_{Az}2}$ and $\boldsymbol{J}_{\theta_{Az}3}$ are

$$\boldsymbol{J}_{\theta_{Az}1}(1,1) = \frac{h_2}{h_1{}^2 + h_2{}^2} - \frac{h_1 h_3}{(h_1{}^2 + h_2{}^2)\sqrt{h_1{}^2 + h_2{}^2 - h_3{}^2}}$$

$$\boldsymbol{J}_{\theta_{Az}1}(2,1) = \frac{-h_1}{h_1{}^2 + h_2{}^2} - \frac{h_2 h_3}{(h_1{}^2 + h_2{}^2)\sqrt{h_1{}^2 + h_2{}^2 - h_3{}^2}}$$

$$\boldsymbol{J}_{\theta_{Az}1}(3,1) = \frac{1}{\sqrt{h_1{}^2 + h_2{}^2 - h_3{}^2}}$$

$$\boldsymbol{J}_{\theta_{Az}2}(1,1) = z_A(l_3{}^2 + kl_3 + p_2 d - p_1 x_A), \ \boldsymbol{J}_{\theta_{Az}2}(1,2) = z_A l_A(k + 2l_3)$$

$$\boldsymbol{J}_{\theta_{Az}2}(1,4) = -l_A p_1 z_A, \ \boldsymbol{J}_{\theta_{Az}2}(1,6) = l_A(l_3{}^2 + kl_3 + p_2 d - p_1 x_A)$$

$$\boldsymbol{J}_{\theta_{Az}2}(2,1) = 2 l_A p_1 y_A, \ \boldsymbol{J}_{\theta_{Az}2}(2,2) = -x_A y_A(k + 2l_3)$$

$$\boldsymbol{J}_{\theta_{Az}2}(2,4) = -y_A(l_3{}^2 + kl_3 + p_2 d), \ \boldsymbol{J}_{\theta_{Az}2}(2,5) = -x_A l_3{}^2 - k x_A l_3 + p_1 l_A{}^2 - p_2 x_A d$$

$$\boldsymbol{J}_{\theta_{Az}2}(3,2) = -l_{Ayz} y_A(d - p_2), \ \boldsymbol{J}_{\theta_{Az}2}(3,3) = y_A(p_2 k - l_3 d + p_2 l_3)$$

$$\boldsymbol{J}_{\theta_{Az}2}(3,5) = l_{Ayz}(p_2 k - l_3 d + p_2 l_3)$$

$$\boldsymbol{J}_{\theta_{Az}2}(1,3) = \boldsymbol{J}_{\theta_{Az}2}(1,5) = \boldsymbol{J}_{\theta_{Az}2}(2,3) = \boldsymbol{J}_{\theta_{Az}2}(2,6) = \boldsymbol{J}_{\theta_{Az}2}(3,1) = \boldsymbol{J}_{\theta_{Az}2}(3,4) = \boldsymbol{J}_{\theta_{Az}2}(3,6) = 0$$

$$\boldsymbol{J}_{\theta_{Az}3}(1,1) = \frac{x_A}{l_A}, \ \boldsymbol{J}_{\theta_{Az}3}(1,2) = \frac{y_A}{l_A}, \ \boldsymbol{J}_{\theta_{Az}3}(1,3) = \frac{z_A}{l_A}$$

$$\boldsymbol{J}_{\theta_{Az}3}(2,1) = \frac{x_A}{l_3 + k}, \ \boldsymbol{J}_{\theta_{Az}3}(2,2) = \frac{y_A}{l_3 + k}, \ \boldsymbol{J}_{\theta_{Az}3}(2,3) = \frac{z_A}{l_3 + k}$$

$$\boldsymbol{J}_{\theta_{Az}3}(3,1) = 0, \ \boldsymbol{J}_{\theta_{Az}3}(3,2) = \frac{y_A}{l_{Ayz}}, \ \boldsymbol{J}_{\theta_{Az}3}(3,3) = \frac{z_A}{l_{Ayz}}$$

where $\boldsymbol{J}_{\theta_{Az}1}(i,j)$ is the element in the i-th row and the j-th column of $\boldsymbol{J}_{\theta_{Az}1}$.

The geometric and inertial parameters of the hybrid robot are listed in Table A1.

Table A1. Geometric and inertial parameters of the hybrid robot.

Parameter	Value	Unit	Parameter	Value	Unit
p_1	845	mm	q_1	480	mm
p_2	360	mm	q_2	205	mm
d	160	mm	k	435	mm
L	180	mm	p_i $(i = 1, 2, 3)$	16	mm
m_i $(i = 1, 2)$	331	kg	m_3	465	kg
m_4	155	kg	m_5	43	kg
e_i $(i = 1, 2)$	650	mm	e_3	653	mm
${}^3\boldsymbol{R}_{C4}$	$[160 \quad 0 \quad 233]^T$	mm	${}^5\boldsymbol{R}_{C5}$	$[0 \quad 0 \quad -12]^T$	mm
$\boldsymbol{I}'_{C1}$	$\begin{bmatrix} 80.73 & 0 & 0 \\ 0 & 81.49 & 5.77 \\ 0 & 5.77 & 4.50 \end{bmatrix}$	kg × m^2	$\boldsymbol{I}'_{C2}$	$\begin{bmatrix} 80.73 & 0 & 0 \\ 0 & 81.49 & -5.77 \\ 0 & -5.77 & 4.50 \end{bmatrix}$	kg × m^2
$\boldsymbol{I}'_{C3}$	$\begin{bmatrix} 284.92 & 0 & 45.98 \\ 0 & 291.91 & 0 \\ 45.98 & 0 & 20.96 \end{bmatrix}$	kg × m^2	$\boldsymbol{I}'_{mi}(i = 1, 2, 3)$	$\begin{bmatrix} 1.33 & 0 & 0 \\ 0 & 1.33 & 0 \\ 0 & 0 & 0.002 \end{bmatrix}$	kg × m^2
$\boldsymbol{I}'_{C4}$	$\begin{bmatrix} 6.33 & 0 & 0 \\ 0 & 5.47 & 0 \\ 0 & 0 & 2.28 \end{bmatrix}$	kg × m^2	$\boldsymbol{I}'_{C5}$	$\begin{bmatrix} 0.414 & 0 & 0 \\ 0 & 0.497 & 0 \\ 0 & 0 & 0.244 \end{bmatrix}$	kg × m^2

References

1. Orsino, R.M.M.; Coelho, T.A.H.; Pesce, C.P. Analytical mechanics approaches in the dynamic modelling of Delta mechanism. *Robotica* **2015**, *33*, 953–973. [CrossRef]
2. Wu, J.; Wang, J.S.; You, Z. An overview of dynamic parameter identification of robots. *Robot. Cim.-Int. Manuf.* **2010**, *26*, 414–419. [CrossRef]
3. Si, G.N.; Chen, F.H.; Zhang, X.P. Comparison of the dynamic performance of planar 3-DOF parallel manipulators. *Machines* **2022**, *10*, 233. [CrossRef]
4. Chanal, H.; Guichard, A.; Blaysat, B.; Caro, S. Elasto-dynamic modeling of an over-constrained parallel kinematic machine using a beam model. *Machines* **2022**, *10*, 200. [CrossRef]
5. Lee, G.; Park, S.; Lee, D.; Park, F.C.; Jeong, J.I.; Kim, J. Minimizing energy consumption of parallel mechanisms via redundant actuation. *IEEE-ASME Trans. Mech.* **2015**, *20*, 2805–2812. [CrossRef]
6. Wu, J.; Gao, Y.; Zhang, B.B.; Wang, L. Workspace and dynamic performance evaluation of the parallel manipulators in a spray-painting equipment. *Robot. Cim.-Int. Manuf.* **2017**, *44*, 199–207. [CrossRef]
7. Merlet, J.P. Determination of the orientation workspace of parallel manipulators. *J. Intell. Robot. Syst.* **1995**, *13*, 143–160. [CrossRef]
8. Karger, A.; Husty, M. Classification of all self-motions of the original Stewart-Gough platform. *Comput. Aided Des.* **1998**, *30*, 205–215. [CrossRef]
9. Luces, M.; Mills, J.K.; Benhabib, B. A review of redundant parallel kinematic mechanisms. *J. Intell. Robot. Syst.* **2017**, *86*, 175–198. [CrossRef]
10. Xu, P.; Cheung, C.F.; Li, B.; Wang, C.; Zhao, C. Design, dynamic analysis, and experimental evaluation of a hybrid parallel-serial polishing machine with decoupled motions. *J. Mech. Robot.* **2021**, *13*, 061008. [CrossRef]
11. Liu, S.; Sun, Y.; Peng, G.; Xue, Y.; Hnydiuk-Stefan, A.; Li, Z. Development of a novel 6-DOF hybrid serial-parallel mechanism for pose adjustment of large-volume components. *Proc. Inst. Mech. Eng. Part C J. Mech. Eng. Sci.* **2021**, *236*, 2099–2114. [CrossRef]
12. Wang, Z.; Li, Y.; Sun, P.; Luo, Y.; Chen, B.; Zhu, W. A multi-objective approach for the trajectory planning of a 7-DOF serial-parallel hybrid humanoid arm. *Mech. Mach. Theory* **2021**, *165*, 104423. [CrossRef]
13. Wu, J.; Yu, G.; Gao, Y.; Wang, L. Mechatronics modeling and vibration analysis of a 2-DOF parallel manipulator in a 5-DOF hybrid machine tool. *Mech. Mach. Theory* **2018**, *121*, 430–445. [CrossRef]
14. Gao, Z.; Zhang, D. Performance analysis, mapping, and multiobjective optimization of a hybrid robotic machine tool. *IEEE Trans. Ind. Electron.* **2015**, *62*, 423–433. [CrossRef]
15. Lai, Y.-L.; Liao, C.-C.; Chao, Z.-G. Inverse kinematics for a novel hybrid parallel–serial five-axis machine tool. *Robot. Cim.-Int. Manuf.* **2018**, *50*, 63–79. [CrossRef]
16. Zhang, J.; Zhao, Y.; Dai, J. Compliance modeling and analysis of a 3-RPS parallel kinematic machine module. *Chin. J. Mech. Eng.* **2014**, *27*, 703–713. [CrossRef]
17. Jin, Y.; Bi, Z.M.; Liu, H.T.; Higgins, C.; Price, M.; Chen, W.H.; Huang, T. Kinematic analysis and dimensional synthesis of Exechon parallel kinematic machine for large volume machining. *J. Mech. Robot.* **2015**, *7*, 041004. [CrossRef]
18. Joshi, S.A.; Tsai, L.-W. The kinematics of a class of 3-DOF, 4-legged parallel manipulators. *J. Mech. Design.* **2003**, *125*, 52–60. [CrossRef]
19. Joshi, S.; Tsai, L.-W. A comparison study of two 3-DOF parallel manipulators: One with three and the other with four supporting legs. *IEEE Trans. Robot. Autom.* **2003**, *19*, 200–209. [CrossRef]

20. Liu, X.-J.; Han, G.; Xie, F.; Meng, Q. A novel acceleration capacity index based on motion/force transmissibility for high-speed parallel robots. *Mech. Mach. Theory* **2018**, *126*, 155–170. [CrossRef]
21. Briot, S.; Caro, S.; Germain, C. Design procedure for a fast and accurate parallel manipulator. *J. Mech. Robot.* **2017**, *9*, 061012. [CrossRef]
22. Merlet, J.P. Solving the forward kinematics of a Gough-type parallel manipulator with interval analysis. *Int. J. Robot. Res.* **2004**, *23*, 221–235. [CrossRef]
23. Kumar, S.; Martensen, J.; Mueller, A.; Kirchner, F. Model simplification for dynamic control of series-parallel hybrid robots—A representative study on the effects of neglected dynamics. In Proceedings of the IEEE/RSJ International Conference on Intelligent Robots and Systems (IROS), Macau, China, 4–8 November 2019.
24. Felis, M.L. RBDL: An efficient rigid-body dynamics library using recursive algorithms. *Auton. Robot.* **2017**, *41*, 495–511. [CrossRef]
25. Li, M.; Huang, T.; Mei, J.; Zhao, X.; Chetwynd, D.G.; Hu, S.J. Dynamic formulation and performance comparison of the 3-DOF modules of two reconfigurable PKM—The Tricept and the TriVariant. *J. Mech. Des.* **2005**, *127*, 1129–1136. [CrossRef]
26. Zhang, H.-Q.; Fang, H.-R.; Jiang, B.-S.; Wang, S.-G. Dynamic performance evaluation of a redundantly actuated and over-constrained parallel manipulator. *Int. J. Autom. Comput.* **2019**, *16*, 274–285. [CrossRef]
27. Shao, H.; Zhang, H.; Yan, W. Dynamic modeling and performance optimization of a 2-PRU-PPRC 2T1R redundant parallel manipulator. In Proceedings of the 9th IEEE Annual International Conference on Cyber Technology in Automation, Control, and Intelligent Systems (IEEE-CYBER), Suzhou, China, 29 July–2 August 2019.
28. Rao, C.; Xu, L.; Chen, Q.; Ye, W. Dynamic modeling and performance evaluation of a 2UPR-PRU parallel kinematic machine based on screw theory. *J. Mech. Sci. Technol.* **2021**, *35*, 2369–2381. [CrossRef]
29. Han, J.; Shan, X.; Liu, H.; Xiao, J.; Huang, T. Fuzzy gain scheduling PID control of a hybrid robot based on dynamic characteristics. *Mech. Mach. Theory* **2023**, *184*, 105283. [CrossRef]
30. Hao, Q. Optimization Design and Dynamic Control of a 2-DoF Planar Parallel Manipulator. Ph.D. Thesis, Tsinghua University, Beijing, China, 2011.
31. Asada, H. A geometrical representation of manipulator dynamics and its application to arm design. *J. Dyn. Syst.-T ASME* **1983**, *105*, 131–142. [CrossRef]
32. Yoshikawa, T. Dynamic manipulability of robot manipulators. *J. Robot. Syst.* **1985**, *2*, 113–124.
33. Chen, M.; Zhang, Q.; Qin, X.; Sun, Y. Kinematic, dynamic, and performance analysis of a new 3-DOF over-constrained parallel mechanism without parasitic motion. *Mech. Mach. Theory* **2021**, *162*, 104365. [CrossRef]
34. Kim, Y.; Desa, S. The definition, determination, and characterization of acceleration sets for spatial manipulators. *Int. J. Robot. Res.* **1993**, *12*, 572–587. [CrossRef]
35. Bowling, A.; Kim, C.H. Dynamic performance analysis for non-redundant robotic manipulators in contact. In Proceedings of the 20th IEEE International Conference on Robotics and Automation (ICRA), Taipei, Taiwan, 14–19 September 2003.
36. Xie, S.; Hu, K.; Liu, H.; Wan, Y. Dynamic modeling and performance analysis of a new redundant parallel rehabilitation robot. *IEEE Access* **2020**, *8*, 222211–222225. [CrossRef]
37. Zhao, Y.J.; Gao, F. Dynamic formulation and performance evaluation of the redundant parallel manipulator. *Robot. Cim.-Int. Manuf.* **2009**, *25*, 770–781. [CrossRef]
38. Ye, H.; Wang, D.; Wu, J.; Yue, Y.; Zhou, Y. Forward and inverse kinematics of a 5-DOF hybrid robot for composite material machining. *Robot. Cim.-Int. Manuf.* **2020**, *65*, 101961. [CrossRef]
39. Zhang, D.; Xu, Y.; Yao, J.; Zhao, Y. Design of a novel 5-DOF hybrid serial-parallel manipulator and theoretical analysis of its parallel part. *Robot. Cim.-Int. Manuf.* **2018**, *53*, 228–239. [CrossRef]
40. Wang, X.J.; Wu, J.; Wang, Y.T. Dynamics evaluation of 2UPU/SP parallel mechanism for a 5-DOF hybrid robot considering gravity. *Robot. Auton. Syst.* **2021**, *135*, 103675. [CrossRef]